

# Three-Coil Wireless Charging System for Metal-Cover Smartphone Applications

Jia-Qi Zhu, Yong-Ling Ban , Yiming Zhang , *Member, IEEE*, Zhengchao Yan , *Student Member, IEEE*, Rui-Min Xu, and Chunting Chris Mi , *Fellow, IEEE*

**Abstract**—A three-coil wireless charging system is proposed for full metal-cover smartphone applications. Considering the space limitation and other antennas in the smartphone, the receiver coil embedded in the smartphone is designed to be miniaturized as 16 mm × 65 mm. By integrating a series capacitance at the end of the 2-mm width narrow horizontal slot loading on the metal cover, the metal cover is converted to a relay coil of the three-coil system and wireless power transfer (WPT) through the metal cover is thus achieved. A prototype of the proposed three-coil system has been built and WPT through metal cover has been validated via experiment. The experimental results show that the prototype achieves 5 W output power with 71% coil-to-coil efficiency.

**Index Terms**—2-mm slot, full metal-cover, miniaturized receiver coil, smartphone application, three-coil system, wireless power transfer.

## I. INTRODUCTION

WIRELESS power transfer (WPT) is a fast developing technology that utilizes electromagnetic field to transfer power wirelessly. Inductive power transfer (IPT) is the most popular WPT technology employing magnetic field coupling [1]. Compared with traditional cord-based charging technique, IPT is more user-friendly and environmental-friendly. With such valuable features, IPT becomes a promising candidate for consumer electronics charging [2]. Because of the rapid expansion of smartphones, achieving WPT in smartphones is now a significant research area.

Manuscript received June 16, 2019; revised August 13, 2019; accepted September 22, 2019. Date of publication September 30, 2019; date of current version February 11, 2020. This work was supported in part by the National Natural Science Foundation of China under Grant 61471098, in part by National Higher-education Institution General Research and Development Project under Grants ZYGX2016J035 and ZYGX2018J037, and in part by China Scholarship Council. Recommended for publication by Associate Editor Yaow-Ming Chen. (Corresponding authors: Yong-Ling Ban; Chunting Chris Mi.)

J.-Q. Zhu is with the School of Electronic Engineering, University of Electronic Science and Technology of China, Chengdu 611731, P. R. China, and also with the Department of Electrical and Computer Engineering, San Diego State University, San Diego, CA 92182 USA (e-mail: jia-qi.zhu@foxmail.com).

Y.-L. Ban and R.-M. Xu are with the School of Electronic Engineering, University of Electronic Science and Technology of China, Chengdu 611731 P. R. China (e-mail: byl@uestc.edu.cn; rmxu@uestc.edu.cn).

Y. Zhang and C. C. Mi are with the Department of Electrical and Computer Engineering, San Diego State University, San Diego, CA 92182 USA (e-mail: zhangym07@gmail.com; mi@ieee.org).

Z. Yan is with the School of Marine Science and Technology, Northwestern Polytechnical University, Xi'an 710072, China, and also with the Department of Electrical and Computer Engineering, San Diego State University, San Diego, CA 92182 USA (e-mail: yanzc1991@gmail.com).

Color versions of one or more of the figures in this article are available online at <http://ieeexplore.ieee.org>.

Digital Object Identifier 10.1109/TPEL.2019.2944845

Until now, most of the previous IPT researches for consumer electronics mainly focus on planar wireless charging [2]–[7], free-positioning wireless charging [8], and multiple receivers [9]–[11]. In [2], a detailed review of planar wireless charging technology for portable electronic products and the Qi standard are indicated. A single-layer winding array with free positioning and localized feature is reported in [8]. A system for multiple mobile receivers with variable lumped capacitances was reported in [10].

The above systems are all designed to operate in free-space condition (FSC). However, in some practical applications, power transfer needs to penetrate through metal barriers, such as metal-cover smartphone wireless charging. Few investigations have been reported in this area. Compared with the smartphone in FSC, metal cover smartphones have the advantages of mechanical robustness and aesthetic appearance, thus designing smartphones with a metal cover becomes a leading trend. However, because the electromagnetic field cannot penetrate through metal barriers, the coupling coefficient of the IPT system will be reduced. Due to the proximity effect caused by the metal cover, the quality factor of the coils will be limited. With a low coupling coefficient and quality factors, the IPT through a metal block usually comes with a low efficiency and low power [12], [13]. Therefore, achieving WPT in a metal-cover smartphone with acceptable performance is an important research area.

The magnetic field generated by the IPT system will induce self-heating and noise current loops in the conductive materials in the smartphone, such as batteries. Because the smartphone is a compact device and the interior space inside the smartphone is limited, the magnetic field distribution of the IPT charging system needs to be investigated. Normally, passive shielding materials like ferrites are integrated below the receiving coil to reduce the magnetic field leakage [14]. A resonant reactive shielding coil is reported in [15], which reduces the magnetic field leakage by producing an opposite magnetic field compared with the incident magnetic field.

An IPT system for metal-cover smartphone is proposed in [16]. A T-slot together with a camera hole and a flash hole is utilized to alter the induced eddy current direction on metal cover. However, certain clearance zone dimension is required because of the requirement to combine the T-slot, the camera hole, and the flash hole. Also, two vertical slots are in connection with the horizontal slot, the camera hole, and the flash hole, which affect the aesthetic appearance of the metal cover and reduce the mechanical robustness. A combined capacitive and inductive

coupler is proposed to achieve WPT across the metal barrier [17]. Two metal plates are employed to induce an ac current on the metal barrier, thus reducing the eddy current loss. The magnetic field is excited by the induced ac current and is picked up by the receiver coil. However, the magnetic field induced by the metal barrier is a horizontal-flux approach. Thus, the receiver coil should be perpendicular to the metal barrier, which does not fit the slim requirement of smartphones. Critically, it cannot be a good candidate for metal-cover smartphone wireless charging.

To enhance the overall performance of the IPT system in the FSC, relay coils can be added between the transmitting coil and receiving coil. A general analysis on domino IPT system is proposed in [18]. Domino resonators in coaxial, circular, and other arrangements are proposed to verify the relay coil IPT system. With an additional relay coil between the transmitting coil and receiving coil, a three-coil system is studied in [19] and the energy efficient of the system is validated to be higher than the two-coil system. However, both of the analyses above neglect the mutual inductance between nonadjacent coils. With regard to metal cover smartphone applications, the distances between the coils are relatively small so that all of the mutual inductances among the three coils need to be taken into consideration. Also, due to the limited quality factor caused by the metal cover, the resistances of the three coils cannot be neglected for circuit analysis.

In this article, a novel three-coil system for metal-cover smartphone wireless charging is proposed. The metal cover is converted from a metal block to a single winding relay coil by connecting a series capacitance at the main horizontal slot, thus significantly enhancing the WPT performance. Besides the ability to achieve WPT for metal-cover smartphone, the proposed receiver coil has a miniaturized size of 15.5 mm × 65 mm, and a much smaller clearance zone (only a narrow horizontal slot of 2 mm × 72.5 mm) as compared with [14] (two side slots, two vertical slots, camera hole, and a flash hole), which meets the leading trends in metal cover smartphone design and becomes a suitable candidate for practical metal-cover smartphone wireless charging. It is noteworthy that the proposed system is also suitable for metal cover smartphones with camera slots and flash holes. The clearance zone of the camera and flashlight will not impact the performance of the wireless charging system.

## II. WORKING PRINCIPLE OF THE RESONANT CIRCUIT

As depicted in Fig. 1, a full-bridge inverter is utilized at the transmitter side of the system to provide ac source power. The transmitter coil, the relay coil, and the receiver coil are magnetically coupled with each other. The metal cover serves as a relay coil. Here, because the distance between the relay coil and the receiver coil is very small (only 1.2 mm), the cross coupling between the transmitter coil and the receiver coil cannot be neglected. Three individual capacitors  $C_1$ ,  $C_2$ , and  $C_3$  are used to resonate with the transmitter coil, the relay coil, and the receiver coil, respectively. To simplify the analysis, the resonating components ( $L_{e1}$ ,  $L_{e2}$ , and  $L_{e3}$ ) and reactance ( $X_1$ ,

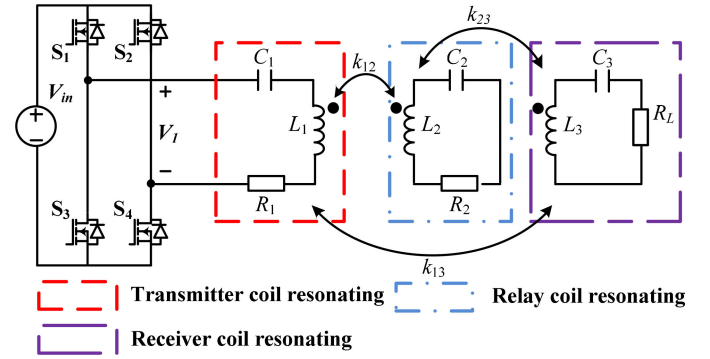


Fig. 1. Circuit model of the proposed three-coil wireless charging system.

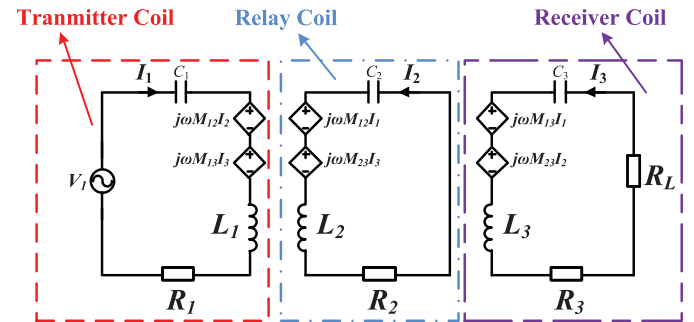


Fig. 2. Simplified fundamental harmonics approximation circuit model of the proposed three-coil wireless charging system.

$X_2$ , and  $X_3$ ) of the three resonating tanks are defined as

$$\begin{cases} j\omega L_1 + \frac{1}{j\omega C_1} + R_1 = L_{e1} = jX_1 + R_1 \\ j\omega L_2 + \frac{1}{j\omega C_2} + R_2 = L_{e2} = jX_2 + R_2 \\ j\omega L_3 + \frac{1}{j\omega C_3} + R_3 = L_{e3} = jX_3 + R_3. \end{cases} \quad (1)$$

With quality factors  $Q_1$ ,  $Q_2$ , and  $Q_3$  of the three coils, the resistances can be derived as

$$R_1 = \frac{\omega L_1}{Q_1}, R_2 = \frac{\omega L_2}{Q_2}, \text{ and } R_3 = \frac{\omega L_3}{Q_3}. \quad (2)$$

It is noteworthy that these resistances are considered in all of the following analyses due to the small quality factor caused by the small size and metal cover. Noticeable difference can be observed between the analyses with and without considering the resistances. For brevity, the comparison results are not shown here.

The fundamental harmonics approximation method is used to analyze the working principle of the circuit topology. The output voltage of the inverter is approximately equivalent to a sinusoidal source. Thus, Fig. 1 is simplified as Fig. 2. Among the transmitter coil, relay coil, and receiver coil, each coil is magnetically coupled with the other two. The magnetic couplings between each two coils are represented by current-controlled voltage sources. By applying Kirchhoff's Voltage Law to the

three resonant tanks in Fig. 2, (3) can be derived:

$$\begin{bmatrix} L_{e1} & j\omega M_{12} & j\omega M_{13} \\ j\omega M_{12} & L_{e2} & j\omega M_{23} \\ j\omega M_{13} & j\omega M_{23} & L_{e3} + R_L \end{bmatrix} \begin{bmatrix} I_1 \\ I_2 \\ I_3 \end{bmatrix} = \begin{bmatrix} V_1 \\ 0 \\ 0 \end{bmatrix}. \quad (3)$$

The currents flowing through the three coils are calculated as (4) at the bottom of the page.

The output power  $P_{\text{out}}$  is calculated as

$$P_{\text{out}} = I_3^2 R_L. \quad (5)$$

By defining  $S$  as (6), the efficiency  $\eta$  is calculated as (7) at the bottom of the page.

$$S = (-\omega^2 M_{12} M_{23} + \omega X_2 M_{13})^2 + (\omega M_{13} R_2)^2 \quad (6)$$

To investigate the voltage on the metal cover, the output power  $P_{\text{out}}$  needs to be fixed as  $P$ . Here, the worst case occurs when people touch across the slot and the maximum  $V_2$  is calculated as

$$\begin{aligned} V_2 &= \left| \frac{I_2}{j\omega C_2} \right| \\ &= \sqrt{[\omega M_{12}(R_3 + R_L)]^2 + (-\omega^2 M_{13} M_{23} + \omega M_{12} X_3)^2} \\ &\quad \sqrt{\frac{P(\omega L_2 - X_2)^2}{S R_L}}. \end{aligned} \quad (8)$$

By defining (9) at the bottom of the page, the input impedance  $Z_{\text{in}}$  of the inductive coupler can be calculated as

$$\begin{cases} a = R_1 R_2 R_3 - X_1 X_2 R_L + R_1 R_2 R_L \\ \quad + \omega^2 (M_{13}^2 R_2 + M_{12}^2 R_3 + M_{12}^2 R_L \\ \quad + M_{23}^2 R_1) - R_3 X_1 X_2 - (R_1 X_2 + R_2 X_1) X_3 \\ b = (R_1 X_2 + R_2 X_1) R_3 - X_1 X_2 X_3 + R_1 R_2 X_3 \\ \quad + (R_1 X_2 + R_2 X_1) R_L - 2\omega^3 M_{12} M_{13} M_{23} \\ \quad + \omega^2 (M_{13}^2 X_2 + M_{12}^2 X_3 + M_{23}^2 X_1) \\ c = R_2 R_L + \omega^2 M_{23}^2 + R_2 R_3 - X_2 X_3 \\ d = (R_3 + R_L) X_2 + R_2 X_3 \end{cases} \quad (9)$$

$$Z_{\text{in}} = \frac{V_1}{I_1} = \frac{ac + bd + j(bc - ad)}{c^2 + d^2}. \quad (10)$$

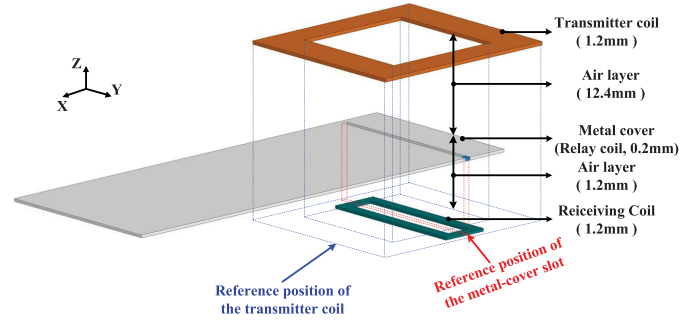


Fig. 3. Breakdown diagram of the proposed three-coil wireless charging system.

The phase angle  $\theta$  of the input impedance  $Z_{\text{in}}$  is thus expressed as

$$\theta = \arctan \frac{bc - ad}{ac + bd}. \quad (11)$$

### III. DESIGN AND STRUCTURE OF THE THREE-COIL INDUCTIVE COUPLER

#### A. Structure of the Three-Coil Inductive Coupler

The breakdown diagram of the proposed three-coil inductive coupler for metal-cover smartphone is shown in Fig. 3. The metal cover is sandwiched between a transmitter coil and a receiver coil via two air layers of thickness 12.4 and 1.2 mm, respectively. For consideration of compactness, AWG 46 Litz-wire of 400 strands is utilized to build the transmitter and receiver coils. The thicknesses of these coils are determined by the Litz-wire diameter, which is 1.2 mm in total.

The plan view of the proposed inductive coupler is shown in Fig. 4. The planar size of the transmitter coil is 66 mm  $\times$  80 mm and the planar size of the miniaturized receiver coil is set to 16 mm  $\times$  65 mm. As for the winding width of the transmitter coil and receiver coil, they are 13.4 and 3.7 mm, respectively. In practical consideration, the planar size of the metal cover is assumed to be 75 mm  $\times$  150 mm. A narrow horizontal slot of size 2 mm  $\times$  72.5 mm is loaded into the metal cover and it is located 14 mm away from the upper edge of the metal cover. To achieve good coupling, both the transmitter coil and the receiver coil are placed symmetrically with the narrow slot. At the left end

$$\begin{cases} I_1 = \frac{(L_{e2}(L_{e3} + R_L) + \omega^2 M_{23}^2) V_1}{(L_{e1} L_{e2} (L_{e3} + R_L) - 2j\omega^3 M_{12} M_{13} M_{23} + \omega^2 M_{13}^2 L_{e2} + \omega^2 M_{12}^2 (L_{e3} + R_L) + \omega^2 M_{23}^2 L_{e1})} \\ I_2 = \frac{(-\omega^2 M_{13} M_{23} - j\omega M_{12} (L_{e3} + R_L)) V_1}{(L_{e1} L_{e2} (L_{e3} + R_L) - 2j\omega^3 M_{12} M_{13} M_{23} + \omega^2 M_{13}^2 L_{e2} + \omega^2 M_{12}^2 (L_{e3} + R_L) + \omega^2 M_{23}^2 L_{e1})} \\ I_3 = \frac{(-\omega^2 M_{12} M_{23} - j\omega M_{13} L_{e2}) V_1}{(L_{e1} L_{e2} (L_{e3} + R_L) - 2j\omega^3 M_{12} M_{13} M_{23} + \omega^2 M_{13}^2 L_{e2} + \omega^2 M_{12}^2 (L_{e3} + R_L) + \omega^2 M_{23}^2 L_{e1})} \end{cases} \quad (4)$$

$$\eta = \frac{I_3^2 R_L}{I_3^2 R_L + I_1^2 R_1 + I_2^2 R_2 + I_3^2 R_3} = \frac{S R_L}{S(R_L + R_3) + \{[X_2(R_3 + R_L) + X_3 R_2]^2 + [-X_2 X_3 + R_2(R_3 + R_L) + \omega^2 M_{23}^2]^2\} R_1 + [(-\omega^2 M_{13} M_{23} + \omega X_3 M_{12})^2 + (\omega M_{12}(R_3 + R_L))^2] R_2} \quad (7)$$



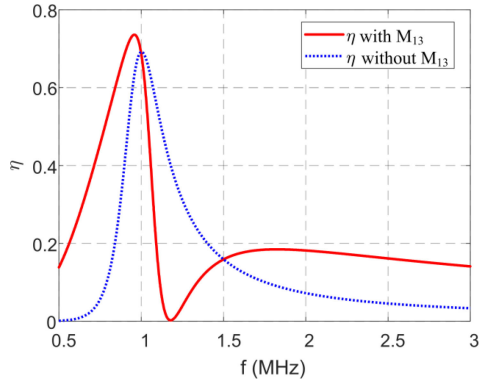


Fig. 7. With 1 MHz resonating frequency, the corresponding efficiency with and without consideration of  $M_{13}$  at different working frequency.

to the negative component “ $-2j\omega^3 M_{12}M_{13}M_{23}$ ” in (4) that is caused by cross coupling between the transmitter coil and receiver coil, the input voltage  $V_1$  will permanently lag behind the input current  $I_1$  and zero voltage switching (ZVS) cannot be achieved. Also, if the resonating frequency of the three resonant tanks is 1 MHz, with measured parameters (inductance and coupling coefficients) of the inductive coupler in Table II, the efficiency  $\eta$  regarding working frequency is plotted based on (7), as shown in Fig. 7. With consideration of  $M_{13}$ , frequency splitting is observed, and the optimum working frequency is smaller than the resonating frequency (1 MHz). Without consideration of  $M_{13}$ , frequency splitting is not occurred, and the optimum working frequency is very close to the resonating frequency (1 MHz). It can be concluded that the frequency splitting in the proposed system is caused by the nonadjacent coupling ( $M_{13}$ ) between the TX coil and Rx coil. According to IEEE C95.1 standard [20], the maximum rms current flowing through human body is 16.7 mA at high-frequency band. Based on [21], the resistance of a human body is about 500  $\Omega$  at high frequency. Thus, the safe rms voltage on the metal cover is required to be lower than 8.35 V [22]. Based on (8), if the working frequency is set at the resonating frequency (1 MHz), the voltage on the metal cover is calculated to be 9.16 V, which does not meet the safety requirement.

Above all, in consideration of  $\eta$ ,  $\theta$ , and  $V_2$ , the working frequency and the resonating frequency of the three resonant tanks cannot be the same, indicating that circuit tuning is necessary to be applied.

### B. Tuning Working Frequency and $C_1$

In this frequency splitting case shown in Fig. 7, either the working frequency or the resonating conditions of the three coils need to be changed to achieve optimum coil-to-coil efficiency. If the working frequency of the system decreases to 0.958 MHz to achieve the optimum coil-to-coil efficiency, the corresponding voltage  $V_2$  on the metal cover is 7.66 V, which meets the safety requirement (8.35 V). The corresponding phase angle  $\theta$  of the input impedance is  $-9.7^\circ$ , indicating that ZVS cannot be achieved. According to (7) and (8), the coil-to-coil efficiency and voltage  $V_2$  do not change with the variation of capacitance  $C_1$ .

Therefore,  $C_1$  can be increased to achieve ZVS. In conclusion, decreasing the working frequency to achieve optimum efficiency and increasing  $C_1$  to achieve ZVS is one optional circuit tuning method.

### C. Tuning Resonant Condition

According to (7),  $C_2$  or  $C_3$  can be tuned to achieve the optimum efficiency. To study the variation of  $C_2$ ,  $L_1$  resonates with  $C_1$  and  $L_3$  resonates with  $C_3$ , leading to  $X_1 = X_3 = 0$ . Equation (7) is thus simplified as

$$\eta = \frac{(-\omega^2 M_{12}M_{23} + \omega X_2 M_{13})^2 R_L + (\omega M_{13}R_2)^2 R_L}{(-\omega^2 M_{12}M_{23} + \omega X_2 M_{13})^2 (R_L + R_3) + [X_2(R_3 + R_L)]^2 R_1 + T}. \quad (12)$$

Here,  $T$  is defined by

$$T = (\omega M_{13}R_2)^2 (R_L + R_3) + [R_2(R_3 + R_L) + \omega^2 M_{23}^2] R_1 + [(-\omega^2 M_{13}M_{23})^2 + (\omega M_{12}(R_3 + R_L))^2] R_2. \quad (13)$$

To achieve the maximum efficiency, equation  $\partial\eta/\partial X_2 = 0$  should be established. Let  $e$ ,  $f$ , and  $g$  be defined by

$$\begin{cases} e = \omega^3 R_1 (R_3 + R_L)^2 M_{12}M_{23}M_{13} \\ f = \omega^2 M_{13}^2 T - [(R_L + R_3)\omega^2 M_{13}^2 + R_1(R_3 + R_L)^2](\omega M_{13}R_2)^2 - R_1(R_3 + R_L)^2(\omega^2 M_{12}M_{23})^2 \\ g = \omega M_{13}(-\omega^2 M_{12}M_{23})[T - (R_L + R_3)(\omega M_{13}R_2)^2]. \end{cases} \quad (14)$$

The optimum  $X_2$  is thus derived as

$$X_{2\_opt} = \frac{-f - \sqrt{f^2 - 4eg}}{2e}. \quad (15)$$

The optimum  $C_2$  is calculated to be

$$C_{2\_opt} = \frac{1}{\omega(\omega L_2 - X_2)}. \quad (16)$$

With  $X_1 = X_3 = 0$ , (8) is simplified as

$$V_2 = \sqrt{[\omega M_{12}(R_3 + R_L)]^2 + (-\omega^2 M_{13}M_{23})^2} \sqrt{\frac{P}{R_L}} \sqrt{\frac{1/\omega C_2}{S}}. \quad (17)$$

Because  $\sqrt{[\omega M_{12}(R_3 + R_L)]^2 + (-\omega^2 M_{13}M_{23})^2} \sqrt{P/R_L}$  is a fixed value,  $\partial(1/\omega C_2)^2/S/\partial C_2$  needs to be solved to obtain the correlation between  $V_2$  and  $C_2$ . Let  $P = \omega^2 M_{13}L_2 - \omega^2 M_{12}M_{23}$ ,  $\partial(1/\omega C_2)^2/S/\partial C_2$  is simplified as

$$\frac{\partial(1/\omega C_2)^2}{\partial C_2} = \frac{-2[(\omega M_{13}R_2)^2 + (P - \frac{M_{13}}{C_2})P]}{\omega C_2 S^2}. \quad (18)$$

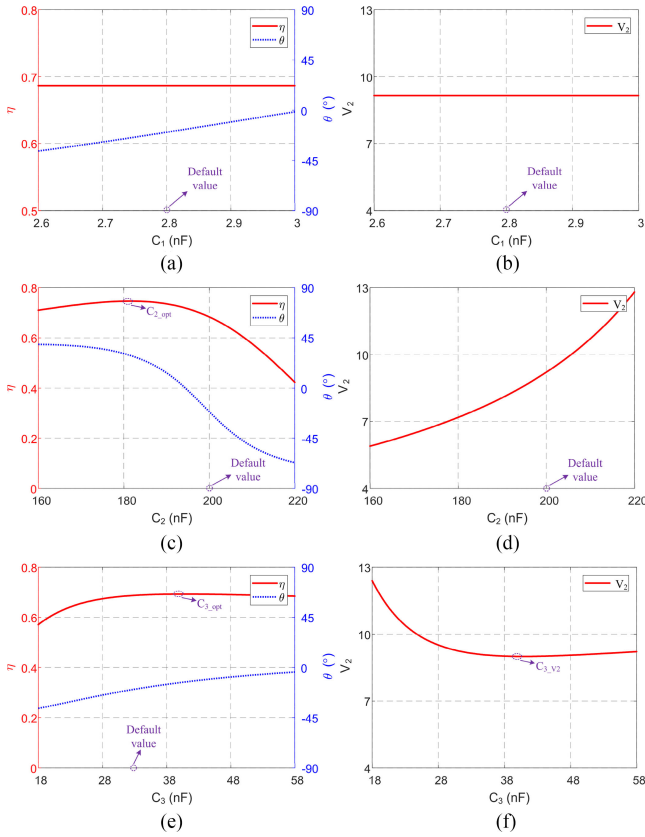


Fig. 8. Calculated (a) efficiencies and phase angle  $\theta$ , (b) voltage  $V_2$  on the metal cover with the variation of capacitance  $C_1$ , (c) efficiencies and phase angle  $\theta$ , (d) voltage  $V_2$  on the metal cover with the variation of capacitance  $C_2$ , (e) efficiencies and phase angle  $\theta$ , and (f) voltage  $V_2$  on the metal cover with the variation of capacitance  $C_3$ .

Let  $\partial(1/\omega C_2)^2/S/\partial C_2 = 0$ ,  $C_{2 \cdot V_2}$  is obtained as

$$C_{2 \cdot V_2} = \frac{M_{13}}{\frac{(\omega M_{13} R_2)^2}{P} + P}. \quad (19)$$

In the proposed three-coil system,  $P > 0$ . Therefore, if  $C_2$  is smaller than  $C_{2 \cdot V_2}$ ,  $V_2$  will be increased with the increase of  $C_2$ . If  $C_2$  is bigger than  $C_{2 \cdot V_2}$ ,  $V_2$  will be decreased with the increase of  $C_2$ .

Similarly, with  $X_1 = X_2 = 0$ , by solving  $\partial\eta/\partial C_3 = 0$  and  $\partial V_2/\partial C_3 = 0$ , the optimum  $C_{3 \cdot \text{opt}}$  for efficiency and  $C_{3 \cdot V_2}$  for smallest  $V_2$  are derived as

$$C_{3 \cdot \text{opt}} = \frac{1}{\omega[\omega L_3 - \frac{\omega^3 R_2 M_{12} M_{13} M_{23}}{(R_2^2 R_1 + \omega^2 M_{12}^2 R_2)}]}, \quad (20)$$

$$C_{3 \cdot V_2} = \frac{1}{\omega^2(L_3 - \frac{M_{13} M_{23}}{M_{12}})}. \quad (21)$$

For better viewing and understanding, the efficiency  $\eta$ , phase angle  $\theta$ , and voltage  $V_2$  regarding  $C_1$ ,  $C_2$ , and  $C_3$  are plotted in Fig. 8. With 1 MHz default resonating frequency, the default value for  $C_1$ ,  $C_2$ , and  $C_3$  are 2.8, 200, and 32.5 nF, respectively. If  $C_1$  is tuned, only the phase angle  $\theta$  will vary. The coil-to-coil efficiency  $\eta$  and  $V_2$  will remain unchanged. If  $C_2$  is tuned, the maximum efficiency will be 74.63%, which is obtained at

TABLE I  
PARAMETERS OF THE INDUCTIVE COUPLER IN DIFFERENT CASES

Parameters	Scheme		
	Case A	Case B	Case C
$k_{12}$	NA	NA	0.1035
$k_{13}$	0.089	0.016	0.095
$k_{23}$	NA	NA	0.228
$L_1$ [ $\mu\text{H}$ ]	9.59	8.70	9.05
$L_2$ [ $\text{nH}$ ]	NA	NA	127.22
$L_3$ [ $\mu\text{H}$ ]	0.89	0.64	0.78
$\eta$	43.97 %	2 %	74.63 %

TABLE II  
EXPERIMENTAL PARAMETERS OF THE PROPOSED THREE-COIL INDUCTIVE COUPLER

Parameter	Value	Parameter	Value
$L_1$	9.05 $\mu\text{H}$	$K_{12}$	0.112
$L_2$	0.127 $\mu\text{H}$	$K_{23}$	0.232
$L_3$	0.78 $\mu\text{H}$	$K_{13}$	0.099
$Q_1$	100	$Q_3$	30
$Q_2$	60	$R_L$	5 $\Omega$

$C_{2 \cdot \text{opt}}$  (181.5 nF). The corresponding  $V_2$  is 7.31 V, which meets the safety voltage requirement. The phase angle  $\theta$  of the input impedance is  $29.2^\circ$ , leading to ZVS. It is noteworthy that  $C_{2 \cdot V_2}$  is calculated to be 270.5 nF, thus the voltage  $V_2$  will be positive correlation with  $C_2$  in Fig. 8(d). If  $C_3$  is tuned, the optimum efficiency will be 69.25%, which is achieved at  $C_{3 \cdot \text{opt}}$  (40.76 nF). The corresponding phase angle  $\theta$  is  $-13^\circ$ , indicating that ZVS cannot be achieved. The smallest  $V_2$  will be obtained when  $C_3$  equals to  $C_{3 \cdot V_2}$  (40.89 nF) and the corresponding voltage is 9 V, which is higher than the safety voltage requirement (8.35 V).

In conclusion, tuning  $C_2$  can achieve the highest efficiency, the smallest corresponding voltage on the metal cover, and ZVS. Compared with the first method that needs to tune both the working frequency and compensating capacitance  $C_1$ , the second method only needs to tune the compensating capacitor  $C_2$  at 1 MHz. Therefore, the experiment was conducted by tuning the compensating capacitor  $C_2$ .

## V. COMPARISON WITH CONVENTIONAL TWO-COIL SYSTEM WITH OR WITHOUT A METAL COVER

For comparison purpose, three cases are investigated, namely, the two-coil system without a metal cover (Case A), the two-coil system with the metal cover as a barrier (Case B), and the proposed three-coil system with the metal cover as a relay coil (Case C). The mutual inductance can be calculated by self-inductance and coupling coefficient as  $M = k\sqrt{L_1 L_2}$ . The inductance and coupling coefficient regarding three cases are listed in Table I for comparison.

As for coupling coefficient  $k_{13}$  between the transmitting coil and receiving coil, case B is very small as 0.016 and Case A is nearly the same as in Case C. That is because the metal cover acts as a metal barrier in case B and the metal cover is transformed to a relay coil by connecting  $C_2$  in Case C. As compared with

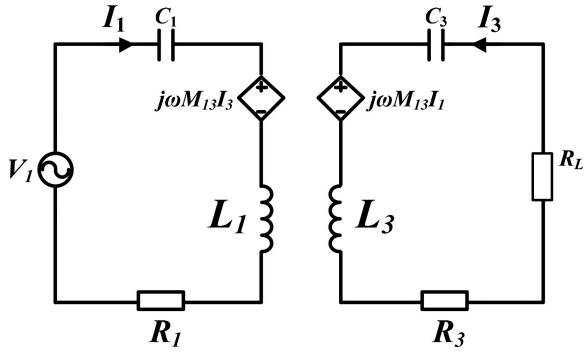
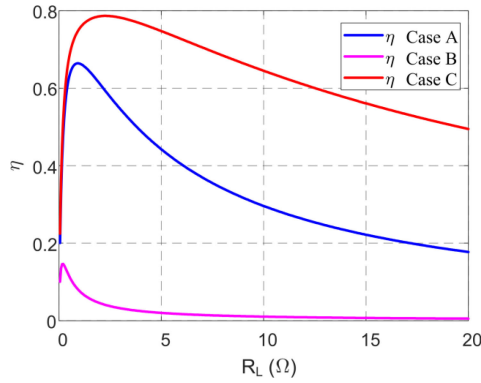


Fig. 9. Equivalent circuit of Case A and Case B.


 Fig. 10. The corresponding efficiency of three cases at different load resistance  $R_L$ .

Case A without the metal cover, both inductances ( $L_1$  and  $L_3$ ) decrease in Case B and Case C. That is because of the proximity effect caused by the metal cover.

To investigate the coil-to-coil charging efficiency, the equivalent circuit of Case A and Case B is shown in Fig. 9. Compensation capacitor  $C_1$  resonates with the transmitting coil and  $C_3$  resonates with the receiving coil, indicating that a series-series (SS) topology is applied. The efficiency  $\eta_{SS}$  for Case A and Case B is calculated as

$$\eta_{SS} = \frac{\omega^2 k_{13}^2 L_1 L_3 R_L}{\omega^2 k_{13}^2 L_1 L_3 R_L + (R_L + R_3)^2 R_1 + (\omega M_{13})^2 R_3}. \quad (22)$$

With the passive parameters (coupling coefficient  $k_{13}$  and inductances  $L_1$  and  $L_3$ ) in Table I, the corresponding coil-to-coil efficiencies for the three cases are calculated by (7) and (22), as shown in Table I. With different load resistance  $R_L$ , the coil-to-coil efficiencies for three cases are depicted in Fig. 10. It can be concluded that the proposed three-coil system achieves the highest efficiency compared with the conventional two-coil system (with or without a metal cover). It is noteworthy that the efficiency of the proposed system is even higher than the two-coil system without a metal cover at the FSC (Case A). That is because the metal cover is converted from a metal barrier to a relay coil and the efficiency of a three-coil system will be higher than a two-coil system.

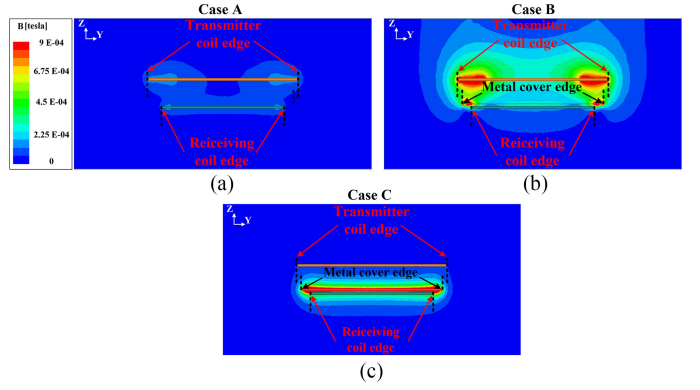
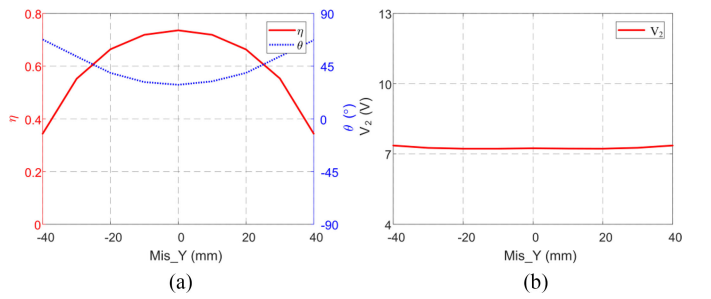


Fig. 11. Magnetic field distribution of the proposed system for (a) Case A, (b) Case B, and (c) Case C.


 Fig. 12. With horizontal misalignment (a) the calculated efficiency  $\eta$ , phase angle  $\theta$ , and (b) the voltage  $V_2$  of the three-coil wireless charging system.

With 5 W output power, the corresponding magnetic field distribution for the three cases are shown in Fig. 11. Among the three cases, magnetic field in Case A is the smallest. As for Case B, the magnetic field concentrates around the transmitting coil. In Case C, the magnetic field concentrates around the metal cover. Therefore, as the metal cover is converted from a metal barrier to a relay coil, the magnetic field will concentrate more around the metal cover rather than the transmitting coil.

## VI. HORIZONTAL AND VERTICAL MISALIGNMENT ANALYSIS

The misalignment of the smartphone includes both the horizontal and vertical misalignments. To analyze the horizontal misalignment, the smartphone (metal cover and receiving coil) is moved along the  $Y$ -axis (coordinate direction is defined in Fig. 3). Because the metal cover (relay coil) and the receiving coil are both integrated in the smartphone, no misalignment exists between them, leading to unchanged coupling coefficient  $k_{23}$ . The coupling coefficients  $k_{12}$  and  $k_{13}$  decrease with the horizontal misalignment. The inductances of the three coils remain unchanged. It is noteworthy that the passive parameters of the inductive coupler are not shown here for brevity. The corresponding coil-to-coil efficiency  $\eta$ , the phase angle  $\theta$ , and voltage  $V_2$  on the metal cover are plotted in Fig. 12. With a horizontal misalignment, the coil-to-coil efficiency  $\eta$  will decrease, the phase angle  $\theta$  will increase, and voltage  $V_2$  will remain unchanged.

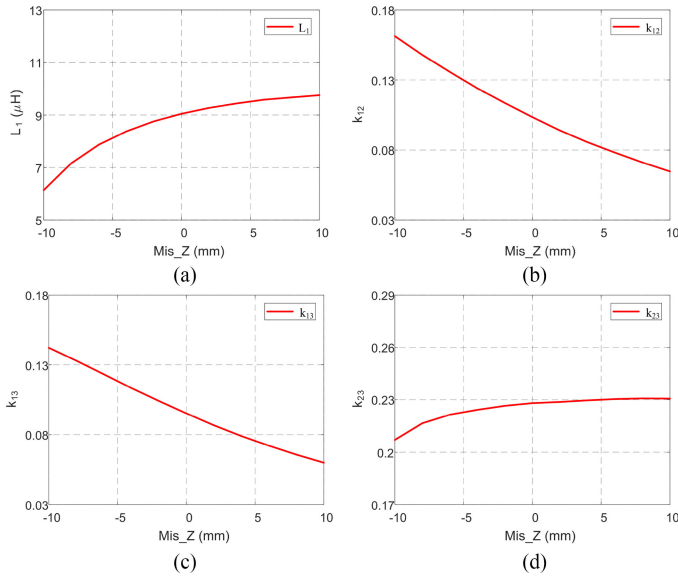


Fig. 13. With vertical misalignment (a) self-inductance  $L_1$  of the transmitting coil, (b) coupling coefficient  $k_{12}$  between the transmitting coil and metal cover, (c) coupling coefficient  $k_{13}$  between the transmitting coil and receiving coil, and (d) coupling coefficient  $k_{23}$  between the metal cover and receiving coil.

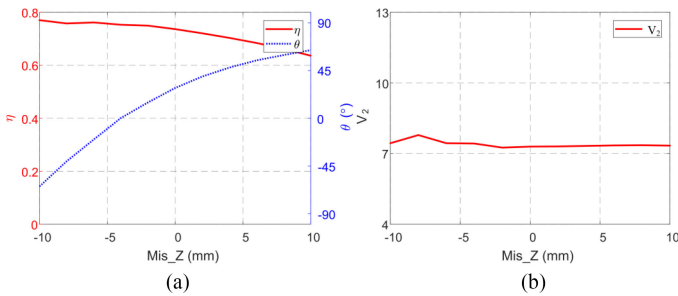


Fig. 14. With vertical misalignment (a) the calculated efficiency  $\eta$ , phase angle  $\theta$ , and (b) the voltage  $V_2$  of the three-coil wireless charging system.

For vertical misalignment, the smartphone is moved along  $Z$ -axis. The corresponding simulated coupling coefficient ( $k_{12}$ ,  $k_{13}$ , and  $k_{23}$ ) and inductances of the transmitter coil ( $L_2$  and  $L_3$  are not shown here for brevity) are shown in Fig. 13. Here, the distance between the transmitter coil and metal cover is defined as  $H$ . With the decrease of  $H$ , the inductance  $L_1$  of the transmitter coil will decrease. That is because the proximity effect of the metal cover with a big surface area on the transmitting coil has a negative correlation with  $H$ . The inductance  $L_2$  of the metal cover and  $L_3$  of the receiving coil remains unchanged. Because the coupling coefficient has a negative correlation with distance between the coils,  $k_{12}$  and  $k_{13}$  increase with the decrease of  $H$  and  $k_{23}$  changes little. With the parameters shown in Fig. 13, the corresponding coil-to-coil efficiency  $\eta$ , the phase angle  $\theta$ , and voltage  $V_2$  are shown in Fig. 14. Different from horizontal misalignment, the efficiency  $\eta$  varies a little and the phase angle  $\theta$  increases with the increase of  $H$ . The voltage  $V_2$  on the metal cover remains unchanged.

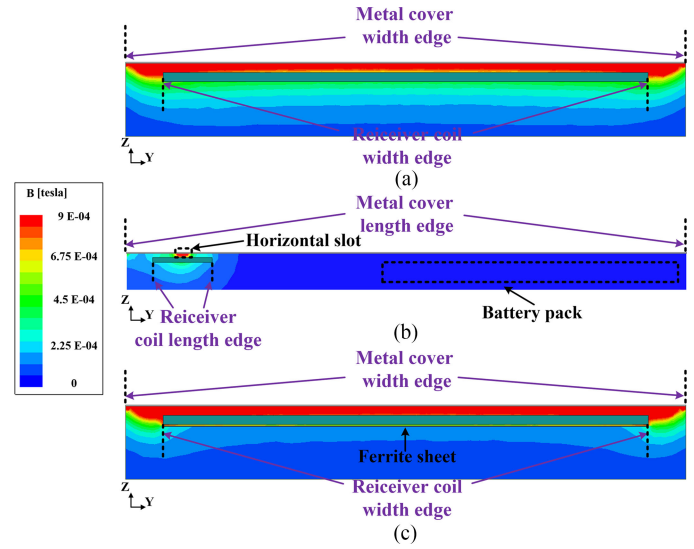


Fig. 15. (a) Front view ( $y$ - $z$ -plane), (b) side view ( $x$ - $z$ -plane) of magnetic field distribution inside the smartphone, and (c) front view ( $y$ - $z$ -plane) of magnetic field distribution inside the smartphone with embedded ferrite sheet.

## VII. ELECTROMAGNETIC INTERFERENCE (EMI) DISCUSSION

The magnetic field generated by the proposed three-coil wireless charging system will cause self-heating and provide noise current loops in conductive materials in the smartphone, which creates EMI issues. Thus, it is important to study the magnetic field distribution within the metal-cover smartphone. However, for different designs of the smartphone, the layout of components inside the smartphone will be different, leading to different EMI conditions. For general analysis, the magnetic strength of the proposed three-coil wireless charging system with a 5 W output power has been simulated, as shown in Fig. 15(a) and 15(b). From Fig. 15(a), it can be seen that the magnetic field is concentrated between the receiving coil and the metal cover, and the magnetic field below the receiving coil is relatively small. As shown in Fig. 15(b), the magnetic field is in close proximity with the 2-mm main horizontal slot of the smartphone and the magnetic field in the remaining area is relatively low. Specifically speaking, in a normal smartphone layout, some of the antennas will be located near the main horizontal slot (concentrated magnetic field area). As for the GPS/WIFI/LTE antennas and others, their operating bands will be higher than 698 MHz (LTE) at ultrahigh-frequency band. Because the working frequency of the proposed wireless charging system is only 1 MHz, there should be no EMI concerns between them. As for big conductive materials like the battery, it is usually implemented at the bottom part of the smartphone, as shown in Fig. 15(b). Because the battery locates far away from the main slot, little EMI exists. With regard to components below the receiving coil, they vary with different smartphone layout. If necessary, a ferrite composite sheet can be placed between the receiving coil and the components. As shown in Fig. 15(c), after integrating a 0.1-mm thick ferrite ( $\mu_r = 200$ , 16 mm  $\times$  65 mm), the magnetic field below the receiving coil is further reduced comparing with Fig. 15(a).

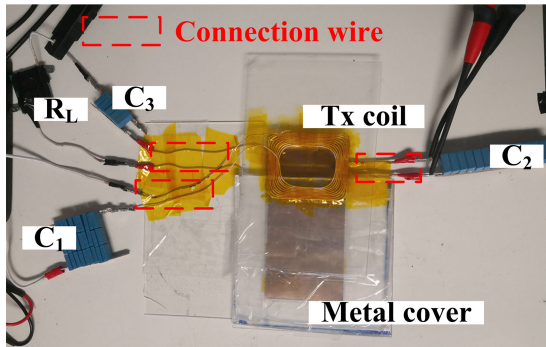


Fig. 16. Fabricated prototype of the proposed three-coil wireless charging system.

## VIII. EXPERIMENT AND DISCUSSION

### A. Measured Parameters of the Fabricated Prototype

The prototype of the proposed three-coil inductive coupler for metal-cover smartphones had been fabricated and tested, as shown in Fig. 16. Within 1 mm, the thickness of the metal cover does not influence the passive parameters of the proposed inductive coupler. Also, the passive parameters of inductive coupler do not vary with the material of the metal cover. Therefore, to successfully conduct the experiment, the metal-cover was actually constructed by gluing 0.2-mm copper sheets onto plexiglass. A slim slot of 2 mm × 72.5 mm was cut on the metal sheet to construct the main horizontal slot. The relay coil was sandwiched by the transmitter coil (TR coil) and the receiver coil (Re coil) via two plexiglass layers of 16 and 1.2 mm, respectively. In consideration of compactness for the wireless charging system, the transmitting coil and receiving coil are both constructed by AWG 46 Litz-wire of 400 strands. The corresponding experimental parameters of the inductive coupler are indicated in Table I. It is noteworthy that the connection Litz-wires for experiment will be removed in practical industrial applications and the practical model will be the same as Figs. 3 and 4.

### B. Experimental Results of the Proposed Three-Coil System

After integrating compensated capacitances  $C_1$  of 2.8 nF,  $C_2$  of 181 nF ( $C_{2,opt}$  to achieve optimum efficiency), and  $C_3$  of 33 nF to the system, the input current  $I_1$ , voltage  $U_2$  on the metal cover, and efficiency  $\eta$  of the system were measured, as shown in Fig. 17. As the output current  $I_3$  varies from 0.4 to 1 A with an increment of 0.2 A (output power from 0.8 to 5 W), voltages  $V_2$  on the metal cover remains under the safety voltage (8.35 V), indicating that the proposed charging system has no safety concerns during the charging process. As depicted in Fig. 17(b), the measured efficiencies are all above 70%. To support the measured results, the experimental waveforms with 5-W output power are shown in Fig. 18. ZVS had been achieved and the rms voltage  $V_2$  on the metal cover is 6.44 V, which is lower than the safety voltage (8.35 V).

With about 22.5 °C indoor temperature, the proposed wireless charging system was operated for 30 min and the corresponding

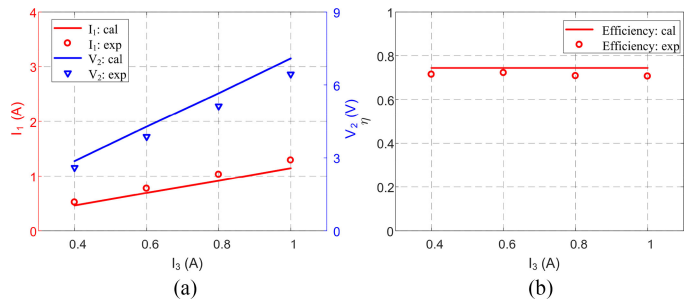


Fig. 17. (a) Measured input current  $I_1$  and voltage  $U_2$  on the metal cover and (b) measured efficiencies at different output currents  $I_3$ .

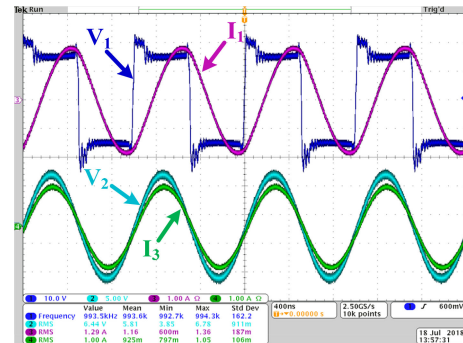


Fig. 18. Experimental waveforms of the proposed three-coil wireless charging system with 5-W output power.

temperature distribution was measured. The highest temperature of the inductive coupler was 26.7 °C and the lowest temperature was 22.6 °C, indicating that the temperature increase of the inductive coupler during wireless charging is negligible. For brevity, the temperature distribution graph is not shown here.

Two methods are proposed in the article to achieve the best performance, namely tuning working frequency and tuning resonant condition. Although the method to tune the working frequency is not adopted in the article, corresponding experiment was conducted to verify the necessity of circuit tuning and significance of cross coupling  $M_{13}$ . Here, the resonating frequencies of the three resonant tanks (Tx coil, relay coil, and Rx coil) are all tuned to 1 MHz. By changing the working frequency from 0.82 to 1.04 MHz with a 10 kHz step, the measured efficiency  $\eta$  with regard to working frequency is plotted, as shown in Fig. 19. It is noteworthy that the upper working frequency of the inverter in our lab is limited to be 1 MHz so that the working frequency beyond 1.04 MHz is not measured. Also, the input voltage lags nearly 90° behind the input current at 0.82 MHz, thus the working frequency below 0.82 MHz is not measured to protect the inverter. It can be observed that the optimum measured efficiency is 0.96 MHz, which is smaller than the resonating frequency of 1 MHz. Also, the voltage  $V_2$  on the metal cover is measured to be 9.13 V at 1 MHz, which does not meet the safety requirement, indicating that the circuit tuning is necessary to be applied. The measured efficiency curve with the variation of working frequency is obviously corresponding to the efficiency curve with  $M_{13}$  rather than the efficiency curve

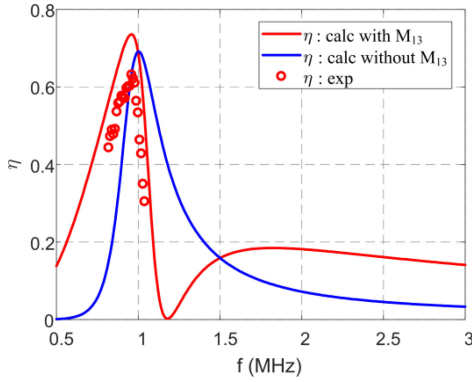


Fig. 19. With 1 MHz resonating frequency, the corresponding measured efficiency and calculated efficiency with and without consideration of  $M_{13}$  at different working frequency.

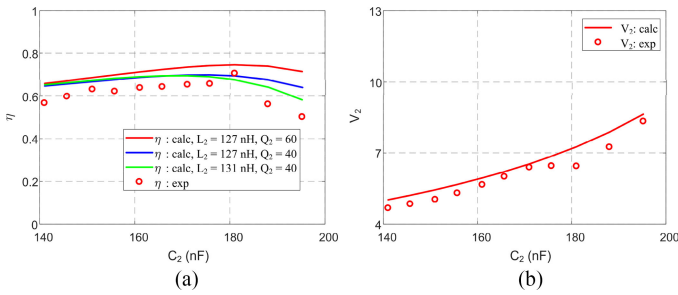


Fig. 20. Calculated and measured (a) efficiencies and (b) voltage  $V_2$  on the metal cover with the variation of capacitance  $C_2$ .

without  $M_{13}$ , validating that the analysis with cross coupling  $M_{13}$  is correct and necessary.

To verify the adopted method of tuning  $C_2$ , the capacitance  $C_1$  and  $C_3$  are selected to be 2.8 and 33 nF, making the Tx coil and Rx coil resonate at 1 MHz. With the variation of capacitance  $C_2$ , the measured efficiency  $\eta$  and voltage  $V_2$  for 5-W output power are shown in Fig. 20(a) and 20(b), respectively. The optimum measured efficiency was achieved with 181 nF compensation capacitance  $C_2$  and the corresponding voltage  $V_2$  was 6.44 V, which met the safety requirement. The measured voltages increase with the increase of capacitance  $C_2$  from 140 to 200 nF. Here, we need to point out that the self-inductance and resistance of the single-turn irregular relay coil (metal cover) is too small to be measured very accurately with an LCR-multimeter or a vector network analyzer, which mainly causes the difference between the calculation curve and experimental curve. Therefore, the calculation efficiency curve with different self-inductance and quality factor are also plotted in Fig. 20(a). With slight decrease of quality factor and increase of  $L_2$ , the measured efficiency curve corresponds better with the calculated efficiency curve with the variation of  $C_2$ .

### C. Discussion of Increasing the Resonating Frequency

Here, the compensated capacitance  $C_2$  is supposed to be integrated into a metal-cover smartphone. We need to admit that the value of  $C_2$  (181 nF) is too big in practical applications. That

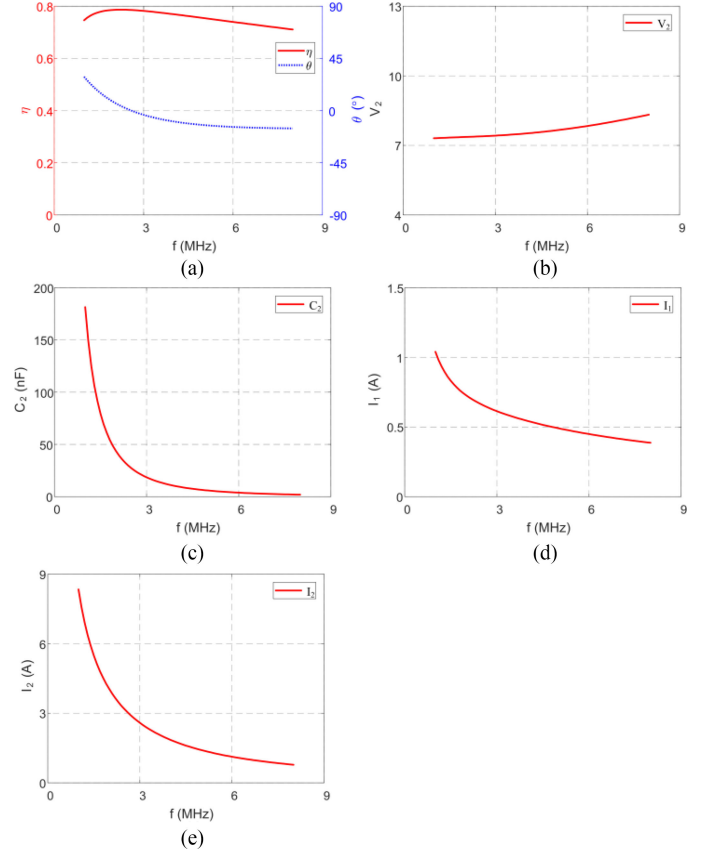


Fig. 21. Calculated (a) efficiencies and phase angle  $\theta$ , (b) voltage  $V_2$  on the metal cover, (c) optimum compensated capacitance  $C_{2,opt}$ , (d) current  $I_1$ , and (e) current  $I_2$  with the variation of working frequency.

is due to the input ac source limitation and available capacitance type of the lab.

If the resonating frequency of the system is increased, and the tuning method and output power remain the same; the corresponding coil-to-coil efficiency  $\eta$ , phase angle  $\theta$  of input impedance, the voltage  $V_2$  on the metal rim, the optimum capacitance  $C_2$ , and the currents  $I_1$  and  $I_2$  are indicated in Fig. 21(a), 21(b), 21(c), 21(d), and 21(e), respectively. Here, it is worth to note that the output current  $I_3$  will remain the same because the output power remains unchanged for fair comparison. As shown in Fig. 21(c), the optimum capacitance  $C_2$  will decrease with the increase of resonating frequency, which helps embed the capacitance into a smartphone. However, with the increase of resonating frequency, the voltage  $V_2$  on the metal cover will increase and the optimum efficiency will decrease, indicating that the frequency cannot be tuned all the way up. Considering the volume of  $C_2$ , the safety issue, and the performance (efficiency) of the proposed three-coil system, the optimum frequency will be 5 MHz. That is because the value of  $C_2$  at 5 MHz is 5.87 nF, which is already reasonable to be embedded into the smartphone. Also, the voltage  $V_2$  on the metal cover is 7.65 V, which is within the safety requirement (8.35 V), and the efficiency is acceptable as 75.5%. As shown in Fig. 21(a), the phase angle  $\theta$  will be negative if the resonating frequency is higher than 2.6 MHz, indicating that ZVS will not be achieved. Based on (11) and

Fig. 8, with the increase of capacitance  $C_1$ ,  $\theta$  will increase and it will not have an influence on the efficiency  $\eta$  and voltage  $V_2$ . Therefore, if the resonating frequency is higher than 2.6 MHz,  $C_2$  needs to be tuned as (16) to achieve the optimum efficiency and  $C_1$  needs to be increased to help achieve ZVS.

## IX. CONCLUSION

In this article, a novel three-coil system for metal-cover smartphone wireless charging is proposed. The three-coil system is composed of a transmitter coil of 66 mm  $\times$  80 mm, a relay coil (metal cover) of 75 mm  $\times$  150 mm, and a miniaturized receiver coil of 16 mm  $\times$  65 mm. By connecting a series capacitor  $C_2$  at the end of the narrow slot, the metal cover is converted to a secondary coil. In consideration of both ZVS and safety issue, the series capacitor  $C_2$  was chosen to be 181 nF to achieve optimum efficiency. As a result, the metal cover is transformed from a magnetic field block to a relay coil and WPT through metal is achieved. The corresponding coil-to-coil efficiency has been is 71% with 5-W output power. Because only a narrow horizontal slot is needed to implement the proposed three-coil system for metal-cover smartphone, the proposed system is reasonable to be integrated into a smartphone in actual applications. In future research, the resonating frequency of the system will be increased to reduce the compensated capacitances.

## REFERENCES

- [1] G. A. Covic and J. T. Boys, "Inductive power transfer," *Proc. IEEE*, vol. 101, no. 6, pp. 1276–1289, Jun. 2013.
- [2] S. Y. Hui, "Planar wireless charging technology for portable electronics products and Qi," *Proc. IEEE*, vol. 101, no. 6, pp. 1290–1301, Jun. 2013.
- [3] J. Park *et al.*, "A resonant reactive shielding for planar wireless power transfer system in smartphone application," *IEEE Trans. Electromagn. Compat.*, vol. 59, no. 2, pp. 695–703, Apr. 2017.
- [4] C. Byungcho, N. Jaehyun, C. Honnyong, A. Taeyoung, and B. Choi, "Design and implementation of low-profile contactless battery charger using planar printed circuit board windings as energy transfer device," *IEEE Trans. Ind. Electron.*, vol. 51, no. 1, pp. 140–147, Feb. 2004.
- [5] Z. N. Low, R. A. Chinga, R. Tseng, and J. Lin, "Design and test of a high-power high-efficiency loosely coupled planar wireless power transfer system," *IEEE Trans. Ind. Electron.*, vol. 56, no. 5, pp. 1801–1812, May 2009.
- [6] X. Zhang, S. L. Ho, and W. N. Fu, "Quantitative analysis of a wireless power transfer cell with planar spiral structures," *IEEE Trans. Magn.*, vol. 47, no. 10, pp. 3200–3203, Oct. 2011.
- [7] L. Xun and S. Y. Hui, "Simulation study and experimental verification of a universal contactless battery charging platform with localized charging features," *IEEE Trans. Power Electron.*, vol. 22, no. 6, pp. 2202–2210, Nov. 2007.
- [8] W. X. Zhong, X. Liu, and S. Y. R. Hui, "A novel single-layer winding array and receiver coil structure for contactless battery charging systems with free-positioning and localized charging features," *IEEE Trans. Ind. Electron.*, vol. 58, no. 9, pp. 4136–4144, Sep. 2011.
- [9] J. J. Casanova, Z. N. Low, and J. Lin, "A loosely coupled planar wireless power system for multiple receivers," *IEEE Trans. Ind. Electron.*, vol. 56, no. 8, pp. 3060–3068, Aug. 2009.
- [10] B. L. Cannon, J. Hoberg, D. D. Stancil, and S. C. Goldstein, "Magnetic resonant coupling as a potential means for wireless power transfer to multiple small receivers," *IEEE Trans. Power Electron.*, vol. 24, no. 7, pp. 1819–1825, Jul. 2009.
- [11] Y. Zhang, T. Lu, Z. Zhao, K. Chen, F. He, and L. Yuan, "Wireless power transfer to multiple loads over various distances using relay resonators," *IEEE Microw. Wireless Compon. Lett.*, vol. 25, no. 5, pp. 337–339, May 2015.
- [12] D. J. Graham, J. A. Neasham, and B. S. Sharif, "Investigation of methods for data communication and power delivery through metals," *IEEE Trans. Ind. Electron.*, vol. 58, no. 10, pp. 4972–4980, Oct. 2011.
- [13] O. Imoru, A. Jassal, H. Polinder, E. Nieuwkoop, J. Tsado, and A. A. Jimoh, "An inductive power transfer through metal object," in *Proc. 1st Int. Future Energy Electron. Conf.*, Tainan, Taiwan, 2013, pp. 246–251.
- [14] S. C. Tang, S. Y. Hui, and H. S.-H. Chung, "Evaluation of the shielding effects on printed-circuit-board transformers using ferrite plates and copper sheets," *IEEE Trans. Power Electron.*, vol. 17, no. 6, pp. 1080–1088, Nov. 2002.
- [15] J. Park *et al.*, "A resonant reactive shielding for planar wireless power transfer system in smartphone application," *IEEE Trans. Electromagn. Compat.*, vol. 59, no. 2, pp. 695–703, Apr. 2017.
- [16] N. S. Jeong and F. Carobolante, "Wireless charging of a metal body device," *IEEE Trans. Microw. Theory Techn.*, vol. 65, no. 4, pp. 1077–1086, Apr. 2017.
- [17] W. Zhou, Y. Su, L. Huang, X. Qing, and P. A. Hu, "Wireless power transfer across metal barrier by combined capacitive and inductive coupling," *IEEE Trans. Ind. Electron.*, vol. 66, no. 5, pp. 4031–4041, May 2019.
- [18] W. Zhong, C. K. Lee, and S. Y. R. Hui, "General analysis on the use of Tesla's resonators in domino forms for wireless power transfer," *IEEE Trans. Ind. Electron.*, vol. 60, no. 1, pp. 261–270, Jan. 2013.
- [19] W. Zhong, C. Zhang, X. Liu, and S. Hui, "A methodology for making a three-coil wireless power transfer system more energy efficient than a two-coil counterpart for extended transfer distance," *IEEE Trans. Power Electron.*, vol. 30, no. 2, pp. 933–942, Feb. 2015.
- [20] IEEE Standards Association, "IEEE standard for safety levels with respect to human exposure to radio frequency electromagnetic fields, 3 kHz to 300 GHz," IEEE, Piscataway, NJ, USA, Rep. no. C95.1.1, 2005.
- [21] International Electrotechnical Commission, "Method of measurement of touch current and protective conductor current," IEC, Geneva, Switzerland, Rep. no. 60990, 1999.
- [22] F. Lu, H. Zhang, and C. Mi, "A two-plate capacitive wireless power transfer system for electric vehicle charging applications," *IEEE Trans. Power Electron.*, vol. 33, no. 2, pp. 964–969, Feb. 2018.



**Jia-Qi Zhu** was born in Henan, China, in 1992. He received the B.S. degree in electronic information science and technology from Southwest Jiaotong University (SWJTU), Chengdu, Sichuan, China, in 2014. Currently he is working toward the Ph.D. degree with the University of Electronic Science and Technology of China (UESTC).

In 2018, he received funding from UESTC and China Scholarship Council, and became a Joint Ph.D. Student in the Department of Electrical and Computer Engineering, San Diego State University, San Diego, CA, USA. His main research interests include near field communication (NFC) and wireless power transfer (WPT) antennas for smartphone applications, especially near field antennas operating with metal-cover smartphones.



**Yong-Ling Ban** was born in Henan, China. He received the B.S. degree in mathematics from Shandong University, Jinan, China, the M.S. degree in electromagnetics from Peking University, Beijing, China, and the Ph.D. degree in microwave engineering from the University of Electronic Science and Technology of China (UESTC), Chengdu, China, in 2000, 2003, and 2006, respectively. In July 2006, he joined the Xi'an Mechanical and Electric Information Institute as a Microwave Engineer. He then joined Huawei Technologies Co., Ltd., Shenzhen, China. At Huawei,

he designed and implemented various terminal antennas for 15 data card and mobile phone products customized from leading telecommunication industries like Vodafone. From September 2010 to July 2016, he was an Associate Professor with UESTC and is currently a Professor with UESTC. From May 2014 to April 2015, he visited the Queen Mary University of London as a Scholar Visitor. His research interests include wideband small antennas for 4G/5G handset devices, MIMO antenna, and millimeter wave antenna array. He is the author of over 60 referred journal and conference papers on these topics. He holds 20 granted and pending Chinese and overseas patents.



**Yiming Zhang** (S'13-M'16) received the B.S. and Ph.D. degrees in electrical engineering from Tsinghua University, Beijing, China, in 2011 and 2016, respectively.

He is currently a Postdoctoral Researcher with San Diego State University, San Diego, CA, USA. His research interests include wireless power transfer for electric vehicles and mobile phones, and resonant converters.



**Rui-Min Xu** (M'07) was born in Sichuan Province, China, in 1958. He received the B.S. and Ph.D. degrees in electromagnetic field and microwave techniques from the University of Electronic Science and Technology of China (UESTC), Chengdu, China, in 1982 and 2007, respectively.

He is currently a Full Professor in UESTC. His current research interests include microwave and millimeter-wave technologies and applications, and radar systems.



**Zhengchao Yan** (S'18) received the B.S. degree in mechanical design, manufacturing and automation from Northwestern Polytechnical University, Xi'an, China, in 2013, where he is currently working toward the Ph.D. degree. He was a Joint Ph.D. Student with San Diego State University, San Diego, CA, USA from 2017 to 2019.

His research interests include wireless power transfer, including electromagnetic field calculation, coil design, and compensation topologies.



**Chunting Chris Mi** (S'00-A'01-M'01-SM'03-F'12) received the B.S.E.E. and M.S.E.E. degrees in electrical engineering from Northwestern Polytechnical University, Xi'an, China, and the Ph.D. degree in electrical engineering from the University of Toronto, Toronto, Ontario, Canada, in 1985, 1988, and 2001, respectively.

He is a Professor and Chair of electrical and computer engineering and the Director of the Department of Energy (DOE)-funded Graduate Automotive Technology Education (GATE) Center for Electric Drive Transportation, San Diego State University, San Diego, CA, USA. Prior to joining SDSU, he was with the University of Michigan, Dearborn from 2001 to 2015.